



Nano FeCoNi-based high-entropy alloy for microwave absorbing with high magnetic loss and corrosion resistance

Zhilin Zhang^a, Jianhui Yuan^{a,*}, Gangjie Lian^c, Sue Ren^d, Yanfang Du^e, Rui Chen^f, Wenbin You^{b,*}, Renchao Che^{b,c,**}

^a School of Materials Science and Engineering, Shanghai University of Engineering Science Shanghai, 201620, China

^b Laboratory of Advanced Materials, Shanghai Key Lab of Molecular Catalysis and Innovative Materials, Academy for Engineering & Technology, Fudan University, Shanghai 200438, China

^c Zhejiang Laboratory, Hangzhou 311100, China

^d AECC Beijing Institute of Aeronautical Materials, Beijing 100095, China

^e AECC Capital Aerospace Machinery corporation Limited, Beijing 100095, China

^f Materials Genome Institute, Shanghai University, Shanghai 200444, China



ARTICLE INFO

Keywords:

FeCoNi alloy
Wet chemical method
Nanometer-scale
Microwave absorption
High permeability
Corrosion resistance

ABSTRACT

With the development of modern communication and military technology, the protection of electromagnetic wave pollution and radar stealth technology have been widely concerned. In this background, the magnetic metals were widely used due to the strong ferromagnetism, which can induce strong magnetic loss to the electromagnetic wave. However, it remains challenging to precisely control the wave-absorbing performance of individual magnetic metals, and there are issues with poor corrosion resistance and high temperature resistance. Therefore, the alloy powders based on Fe, Co, and Ni in this work were prepared by wet chemical method at room temperature. Different from most of the traditional powder metallurgy methods, the wet chemical method enables us to obtain binary, ternary and quaternary alloys with a nanometer-scale and uniform distribution, all products have a microscopic morphology of 300–500 nm spheres. The FeCoNi alloy powder shows an effective absorption band ($RL < -10$ dB) of 7 GHz in the high frequency electromagnetic wave range at an ultrathin thickness of 1.5 mm, which has a high temperature magnetism ($T_c > 900$ K) and excellent corrosion resistance. Further doping of Cu to form a quaternary alloy can improve the corrosion resistance and maintain the original wave-absorbing properties, while doping of Mo and Sn can adjust the position of the effective absorption bandwidth.

1. Introduction

With the advent of the 5G mobile network era and the development of artificial intelligence and military technology, various electronic devices produce more and more electromagnetic radiation, electromagnetic pollution has become the fourth pollution after air pollution, water pollution and noise pollution [1–3]. Relevant research indicates that electromagnetic radiation can cause serious interference to communication equipment and electronic instruments, even cause electrical leakage and explosion risk, and human health can be adversely affected by prolonged exposure to high levels of radiation [4,5]. Therefore, it is

increasingly important to find electro-magnetic absorber (EMA) with excellent performance. In terms of current practical applications, traditional ferrite and commercial carbonyl iron powder have the problems of single magnetic loss mode, narrow effective absorption bandwidth (EAB), high density, poor corrosion resistance and high temperature resistance [6–12]. Magnetic metals are usually highly magnetic and conductive, both magnetic and dielectric losses for electromagnetic waves, and have excellent wave-absorbing properties in the high-frequency microwave band, so the magnetic metals have become the main research direction for EMA. However, magnetic metals such as iron monomer face the problem of poor high temperature resistance and

* Corresponding authors.

** Corresponding author at: Laboratory of Advanced Materials, Shanghai Key Lab of Molecular Catalysis and Innovative Materials, Academy for Engineering & Technology, Fudan University, Shanghai 200438, China.

E-mail addresses: yuanjh@sues.edu.cn (J. Yuan), wbyou@fudan.edu.cn (W. You), rcche@fudan.edu.cn (R. Che).

corrosion resistance, and it is often difficult to achieve the original microwave absorption performance in practical applications.

In order to improve the high-temperature magnetism and corrosion resistance of magnetic metals, alloying can be adopted to improve the stability in practical applications. Moreover, high-entropy alloys inhibit the formation of intermetallic compounds due to lattice distortion, thus strengthening of the crystal structure improves the resistance of corrosion [13–16]. For the alloy powders used for microwave absorption, the existing research is mostly binary alloys and ternary alloys, with large particle size and uneven particle size distribution, resulting in poor absorption performance of electromagnetic waves. The uniform and small-scale metal particles allow sufficient multiple reflections of electromagnetic waves in them, which increases the ability of electromagnetic wave loss. Moreover, when the particles are refined to nanoscale size, the specific surface area of the absorber gets increased, thus the interfacial polarization effect can be enhanced, and the polarization relaxation of the atoms on the surface of the particles also improve the wave-absorbing performance. Therefore, nano-sized magnetic metal alloys are the required for medium and high entropy magnetic alloys [17–19].

Therefore, the binary alloys FeCo, CoNi, and FeNi, the ternary alloy FeCoNi, and the quaternary alloys FeCoNiCu, FeCoNiMo, and FeCoNiSn have been prepared by the same method with ferromagnetic metals Fe, Co, and Ni as substrates. This method can be widely used for the preparation of magnetic metal alloy powders, and the powder particles prepared by the liquid phase have a uniform particle size distribution and are more controllable than dry methods such as ball milling, spraying and atomization. And the prepared samples have a strong saturation magnetization strength, which can cause a large number of eddy current loss and ferromagnetic resonance loss in the X-band and Ku-band [20–27]. The alloy particles produced in this paper are all on the nanoscale, mostly between 300 nm and 500 nm, and have superior wave-absorbing properties compared to some micrometer-scale alloy powders [28–31]. The FeCoNi alloy powder has excellent corrosion resistance due to high-entropy alloying, and the Curie temperature of

900 K or more allows it to maintain wave-absorbing properties in high-temperature scenarios. And by doping trace Cu into the FeCoNi lattice, the corrosion resistance is further strengthened compared with the original FeCoNi, and the doping of Mo and Sn can move the EAB to correspond to the microwave absorption requirements of different frequency bands. In addition, the resistivity of the alloyed material is higher than single element metals, which is conducive to establishing a proper impedance match and generating more polarization relaxation loss after electromagnetic wave enters the medium, so the microwave absorption performance will also be improved [32,33].

2. Experimental section

2.1. Materials and fabrication

2.1.1. Materials

Ferrous sulfate heptahydrate ($\text{FeSO}_4 \cdot 7\text{H}_2\text{O}$), cobalt sulfate heptahydrate ($\text{CoSO}_4 \cdot 7\text{H}_2\text{O}$), nickel chloride hexahydrate ($\text{NiCl}_2 \cdot 6\text{H}_2\text{O}$), sodium hydroxide (NaOH), copper sulfate anhydrous (CuSO_4), stannous chloride tetrahydrate ($\text{SnCl}_2 \cdot 4\text{H}_2\text{O}$), ammonium molybdate tetrahydrate ($(\text{NH}_4)_6\text{Mo}_7\text{O}_{24} \cdot 4\text{H}_2\text{O}$), and hydrazine hydrate ($\text{N}_2\text{H}_4 \cdot \text{H}_2\text{O}$) are all from Sinopharm Chemical ReagentCo., Ltd. Deionized water from a Milli-Q system (Millipore, Bedford, MA) was used in all experiments.

2.1.2. Preparation of binary alloys

Three binary alloys, FeCo, CoNi and FeNi, were prepared by liquid phase reduction method at room temperature, in which the component feeding ratio was 1: 1. $\text{FeSO}_4 \cdot 7\text{H}_2\text{O}$, $\text{CoSO}_4 \cdot 7\text{H}_2\text{O}$ and $\text{NiCl}_2 \cdot 6\text{H}_2\text{O}$ were divided in pairs, and 12 mmol of each was dissolved in 100 mL deionized water into three cups of salt solution (FeCo, CoNi, FeNi), another 22 g NaOH was dissolved in 20 mL of deionized water and mixed with 45 mL of $\text{N}_2\text{H}_4 \cdot \text{H}_2\text{O}$ (85 wt%), then slowly add the above prepared hydrazine hydrate solution to the vigorously stirred metal salt solution, and react in the agitation for 24 hours. Finally, the samples in the three cups were collected by magnetic absorption method, cleaned three times each with

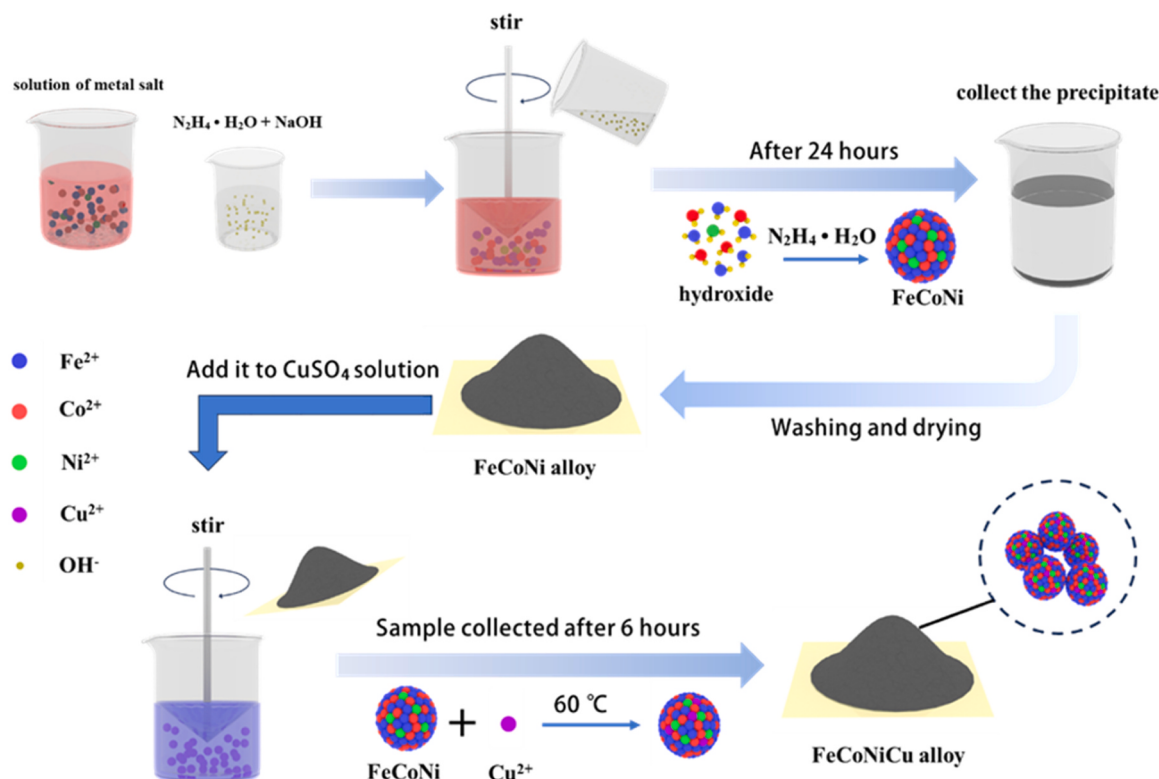


Fig. 1. Schematic illustration for the preparation of FeCoNiCu.

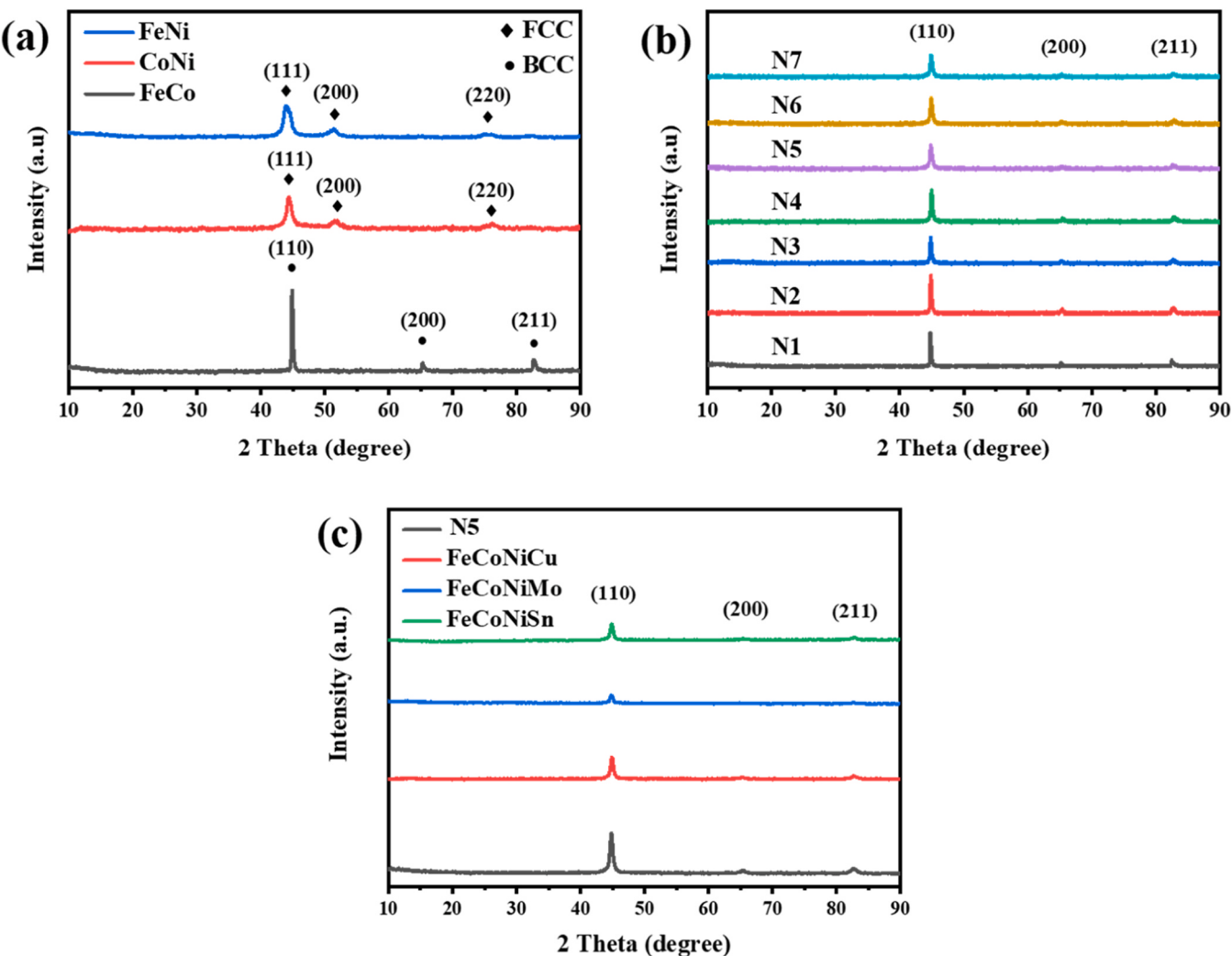


Fig. 2. (a) XRD pattern of FeCo, CoNi, and FeNi; (b) XRD pattern of Fe₅Co₄Ni_{4-x} ($x = 0, 0.25, 0.5, 0.75, 1, 1.25, 1.5$); (c) XRD pattern of FeCoNi, FeCoNiCu, FeCoNiMo, and FeCoNiSn.

deionized water and anhydrous ethanol, and the obtained sample powder was dried in the oven at 70 °C.

2.1.3. Preparation of FeCoNi alloy

The Fe₅Co₄Ni alloy powder was synthesized by a similar method, 8 mmol FeSO₄·7H₂O, 6.4 mmol CoSO₄·7H₂O, 1.6 mmol NiCl₂·6H₂O were dissolved in 66 mL deionized water, and 13 g NaOH was added into 26 mL deionized water and mixed with 20 mL N₂H₄·H₂O (85 wt%), the prepared N₂H₄·H₂O (85 wt%) was added to the FeCoNi salt solution under vigorous stirring and reacted for 24 hours. The samples were collected by magnetic method, cleaned three times each with deionized water and anhydrous ethanol, and the obtained sample powder was dried in the oven at 70 °C. Fe₅Co₄Ni_x ($x = 0, 0.25, 0.5, 0.75, 1, 1.25, 1.5$) was prepared in total by adjusting the addition of NiCl₂·6 H₂O. Fe₅Co₄, Fe₅Co₄Ni_{0.25}, Fe₅Co₄Ni_{0.5}, Fe₅Co₄Ni_{0.75}, Fe₅Co₄Ni, Fe₅Co₄Ni_{1.25}, and Fe₅Co₄Ni_{1.5} were named as N1, N2, N3, N4, N5, N6, and N7 respectively.

2.1.4. Preparation of quaternary alloys

5% CuSO₄ solution 100 mL, 5% (NH₄)₆Mo₇O₂₄·4H₂O solution 100 mL, and 5% SnCl₂·4H₂O solution 100 mL were prepared. To the above three solutions were added 1 g Fe₅Co₄Ni, respectively, at 60 degrees, 70 degrees, 90 degrees water bath conditions to react 6 h, the sample powder obtained in the oven at 70 degrees drying.

2.2. Characterization

X-ray diffractometer (XRD, Bruker, Germany, D8-Advance) was used for qualitative analysis of crystal phase composition and crystallinity, and field emission scanning electron microscope (SEM, Hitachi S-4800, Japan) was used to observe the micromorphology of the sample, the magnetic properties of the sample were tested using a low magnetic measurement system (MPMS SQUID VSM, Quantum Design Company, USA) at a temperature of 300 K, and the change in magnetization strength of FeCoNi and FeCoNiCu has been measured in a constant magnetic field of 100 Oe and at temperatures of 350–1000 K. The sample was mixed with paraffin at a ratio of 7:3, mix evenly in proportion and press into a ring with an inner diameter of 3.04 mm, an outer diameter of 7 mm and a thickness of 2–3 mm. Test the electromagnetic parameters of the sample within 2–18 GHz frequency with vector network analyzer (N5230C, Keysight Company, USA). Corrosion tests are based on salt water immersion experiments and electrochemical measurements. The salt water immersion experiments use 100 mL of 3.5% NaCl solution to soak the sample for six months. Electrochemical measurements were performed with the electrochemical workstation (AUTOLAB PGSTAT302N) equipped with a three-electrode battery unit. A glassy carbon electrode with an area of 0.125 cm² was used as the working electrode, a carbon rod was utilized as the counter electrode, and AgCl was employed as the reference electrode, the 3.5%

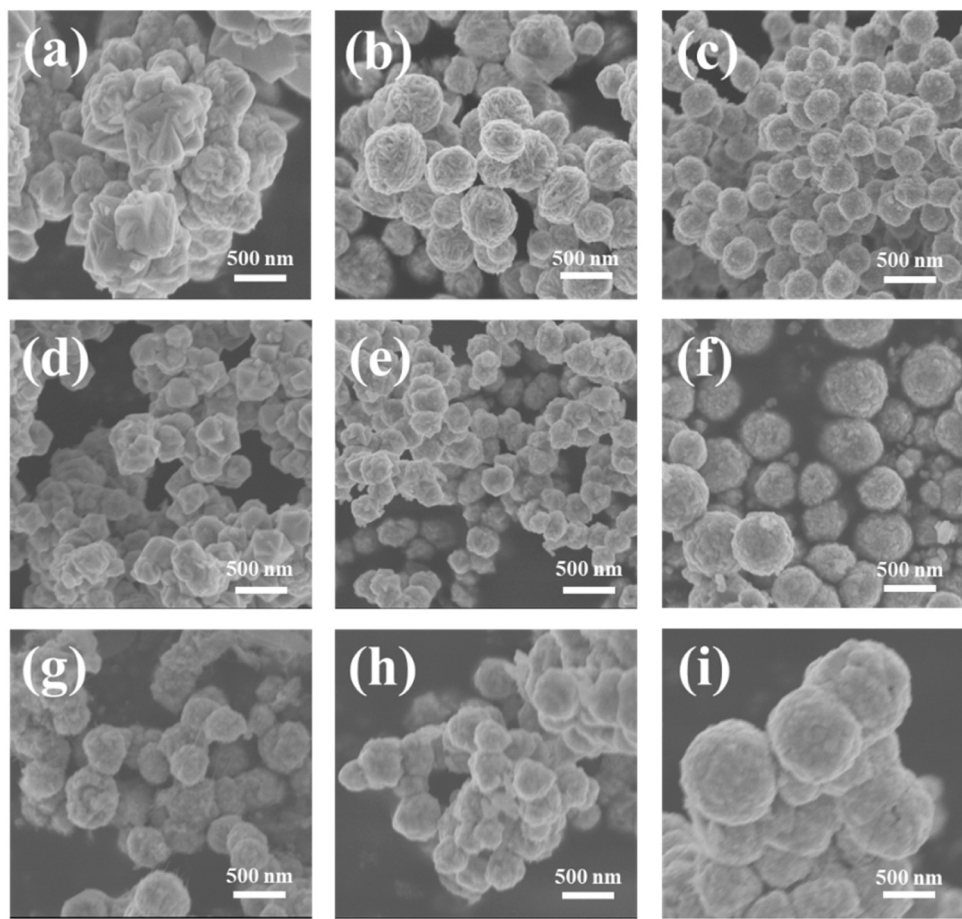


Fig. 3. (a-c) SEM images of (a) FeCo, (b) CoNi, and (c) FeNi; (d-f) SEM images of (d) N2, (e) N5, and (f) N7; (g-i) SEM images of (g) FeCoNiCu, (h) FeCoNiMo, and (i) FeCoNiSn.

NaCl solution was chosen as electrolyte. The scan rate for potentiodynamic polarization measurements was set to 1 mV/s with a voltage range of $-1.5 \text{ V} \sim 1 \text{ V}$. EIS results were obtained in the frequency range of 100 kHz to 0.01 Hz.

3. Results and discussion

3.1. Synthesis and phase analysis

Fig. 1 shows the preparation process of the samples in this paper by illustrated with the synthesis of FeCoNiCu. The synthesis of FeCoNi alloys involves the formation of Fe, Co, and Ni hydroxides, then it was gradually reduced to the alloy by hydrazine hydrate, and then the obtained FeCoNi was incorporated into CuSO₄ solution for substitution reaction to finally obtain FeCoNiCu alloy.

XRD test results were used to analyze the phase composition of the samples. **Fig. 2a** shows the XRD patterns of FeCo, CoNi and FeNi binary alloys. It can be analyzed that the prepared FeCo has three obvious diffraction peaks which correspond to the (110), (200), and (211) crystal planes respectively, and it accurately corresponds to the FeCo alloy phase (PDF#44-1433) with a body-centered cubic (BCC) structure by database comparison. CoNi and FeNi have similar XRD patterns, in which their three diffraction peaks correspond to the (111), (200), and (220) crystal planes of the face-centered cubic (FCC) Ni (PDF#70-1849) and FeNi₃ (PDF#65-3244), respectively. It can be concluded that the addition of Ni transforms the BCC structure of FeCo into the FCC structure of Ni, which is more directly verified by the XRD patterns (**Fig. S1**) of FeCoNi (1:1:1) in the [supplementary materials](#). Through the analysis of XRD images combined with the schematic illustration

(**Fig. 1**). From the XRD results, it is concluded that FeCo possesses BCC structure, however, CoNi and FeNi prepared by the same method exhibit FCC structure. A mixed solution of NaOH and hydrazine hydrate was used in the experiment to reduce the metal ions in solution, and the process is that OH⁻ combines with the metal ions in solution to form hydroxide first, and then a part of the hydroxide is reduced to core first, and then grows up gradually to form the nano-microsphere alloys finally. The analysis of above results leads to the conclusion that OH⁻ reacts first with Ni²⁺ in CoNi and FeNi solutions to form Ni(OH)₂ precipitate. Because the solubility product of Ni(OH)₂ ($K_{sp} = 2 \times 10^{-15}$) is smaller than the solubility product constant of Fe(OH)₂ and Co(OH)₂, it tends to form Ni(OH)₂ solid state. Subsequently, Ni(OH)₂ was first reduced by N₂H₄ • H₂O to form the core of Ni, and CoNi and FeNi nanoparticles with FCC structure were grown with Ni as the core. While in FeCo solution Fe(OH)₂ and Co(OH)₂ are directly reduced to form the BCC structure of FeCo.

Fe₅Co₄Ni_x ($x = 0.25, 0.5, 0.75, 1, 1.25, 1.5$) alloy powders were prepared by adding a small amount of Ni element on the basis of FeCo alloys by a similar method. As shown in **Fig. 2b**, all six FeCoNi samples with a small amount of Ni added still maintain the BCC structure of the original FeCo, and the positions of the diffraction peaks compared to the original FeCo are able to correspond neatly. Since the concentration of Ni ions in the solution is now much lower than that of Fe and Co ions, it is still preferred that the hydroxides of Fe and Co are formed first, and then the reduced products of the FeCo crystal structure are obtained.

On the basis of sample N5, the FeCoNiCu, FeCoNiMo and FeCoNiSn alloys were obtained by replacing the sample with 5% CuSO₄ solution, 5% (NH₄)₆Mo₇O₂₄ • 4H₂O solution and 5% SnCl₂ • 4H₂O solution. **Fig. 2c** shows that they have no change in the position of the diffraction

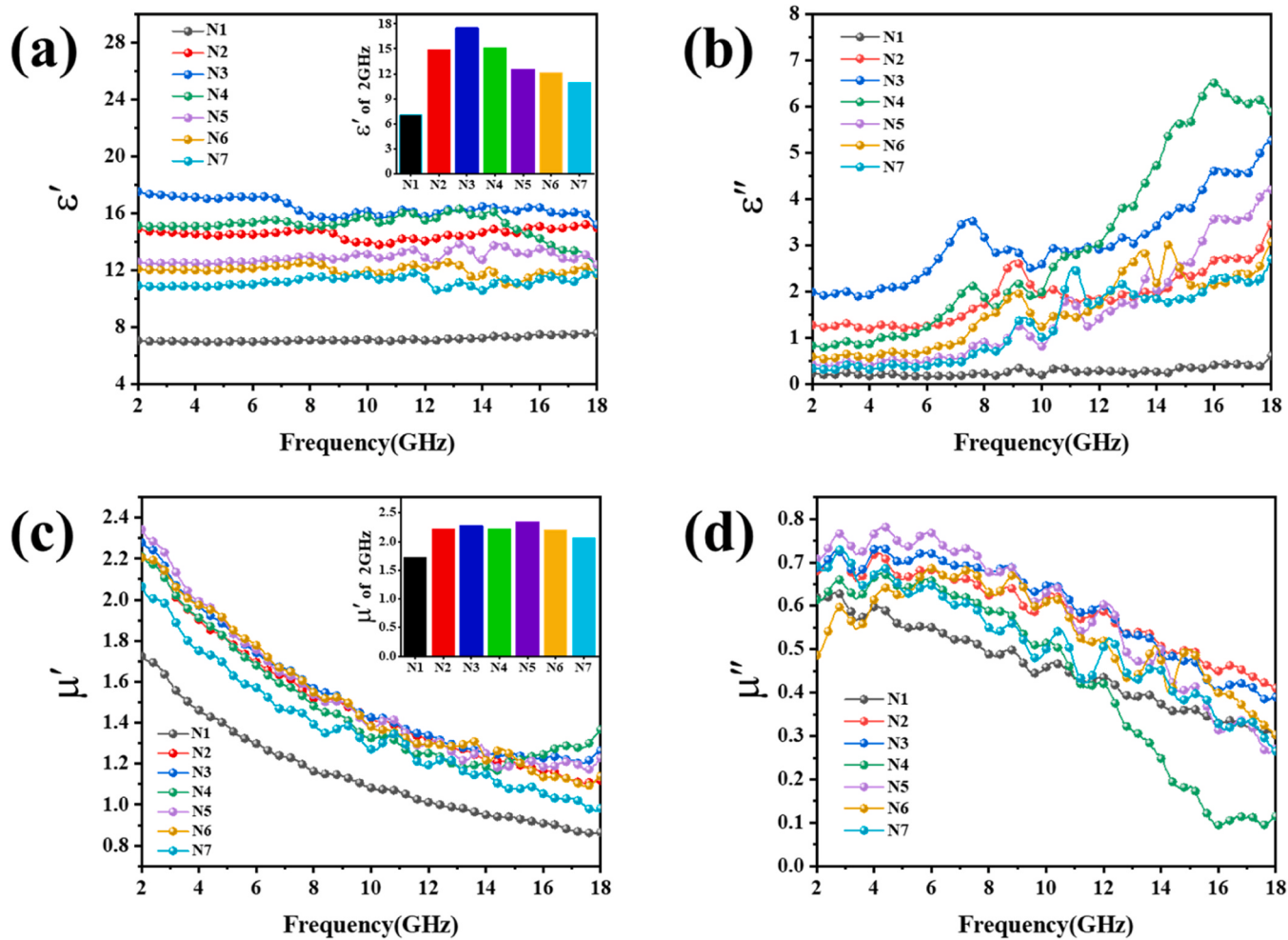


Fig. 4. (a) Real part permittivity, (b) imaginary part permittivity, (c) real part permeability, and (d) imaginary part permeability of $\text{Fe}_5\text{Co}_4\text{Ni}_x$ ($x = 0, 0.25, 0.5, 0.75, 1, 1.25, 1.5$).

peaks relative to the original N5, which is still a BCC structure of FeCo. The nano alloy powders (N5) are not completely displaced or encapsulated by the metal on the surface of the particles but enter the crystal structure to form an alloy when they are dispersed in a metal salt solution with a backward metal activity. It should be the special property brought by alloying, which also reflects that the nano alloy powders prepared by this method possesses excellent corrosion resistance.

3.2. Microscopic morphology

Fig. 3a shows the FeCo alloy as large particles with a slight degree of agglomeration. **Fig. 3b** is CoNi alloy showing distinct spherical particles with a scale distribution around 500 nm. And **Fig. 3c** is FeNi alloy with obvious spherical particles with scale distribution of about 300 nm and some protrusions on the surface. It can be shown that alloys formed by Ni with Fe, Co can form nanospherical particles with excellent dispersion.

Fig. 3(d-f) shows the microscopic morphology of N2, N5 and N7 presented as a spherical shape with a particle size of about 400 nm, and with the increase of Ni content the shape is closer to the standard spherical shape, and the size of the particle increases accordingly. Therefore, it can be analyzed that the addition of a small amount of Ni can make the original irregular FeCo particles have a spherical morphology, and the addition of Ni content will also have an effect on the regularity and size of the ball. **Fig. 3(g-i)** shows the microscopic morphology of FeCoNiCu, FeCoNiMo and FeCoNiSn, respectively, which

basically maintains the nano-spherical shape of the original FeCoNi alloy.

3.3. Electromagnetic properties and wave absorption performance

The electromagnetic parameters of $\text{Fe}_5\text{Co}_4\text{Ni}_x$ ($x = 0, 0.25, 0.5, 0.75, 1, 1.25, 1.5$) were compared and analyzed. In addition, the electromagnetic properties of FeCoNiCu, FeCoNiMo, and FeCoNiSn are discussed. According to the transmission line theory, the formulas of impedance matching Z and reflection loss RL are as follows [34]:

$$Z = \sqrt{\frac{\mu_r}{\epsilon_r}} \tanh \left[j \left(\frac{2\pi f d}{c} \right) \sqrt{\mu_r \epsilon_r} \right] \quad (1)$$

$$RL = 20\log \left| \frac{Z-1}{Z+1} \right| \quad (2)$$

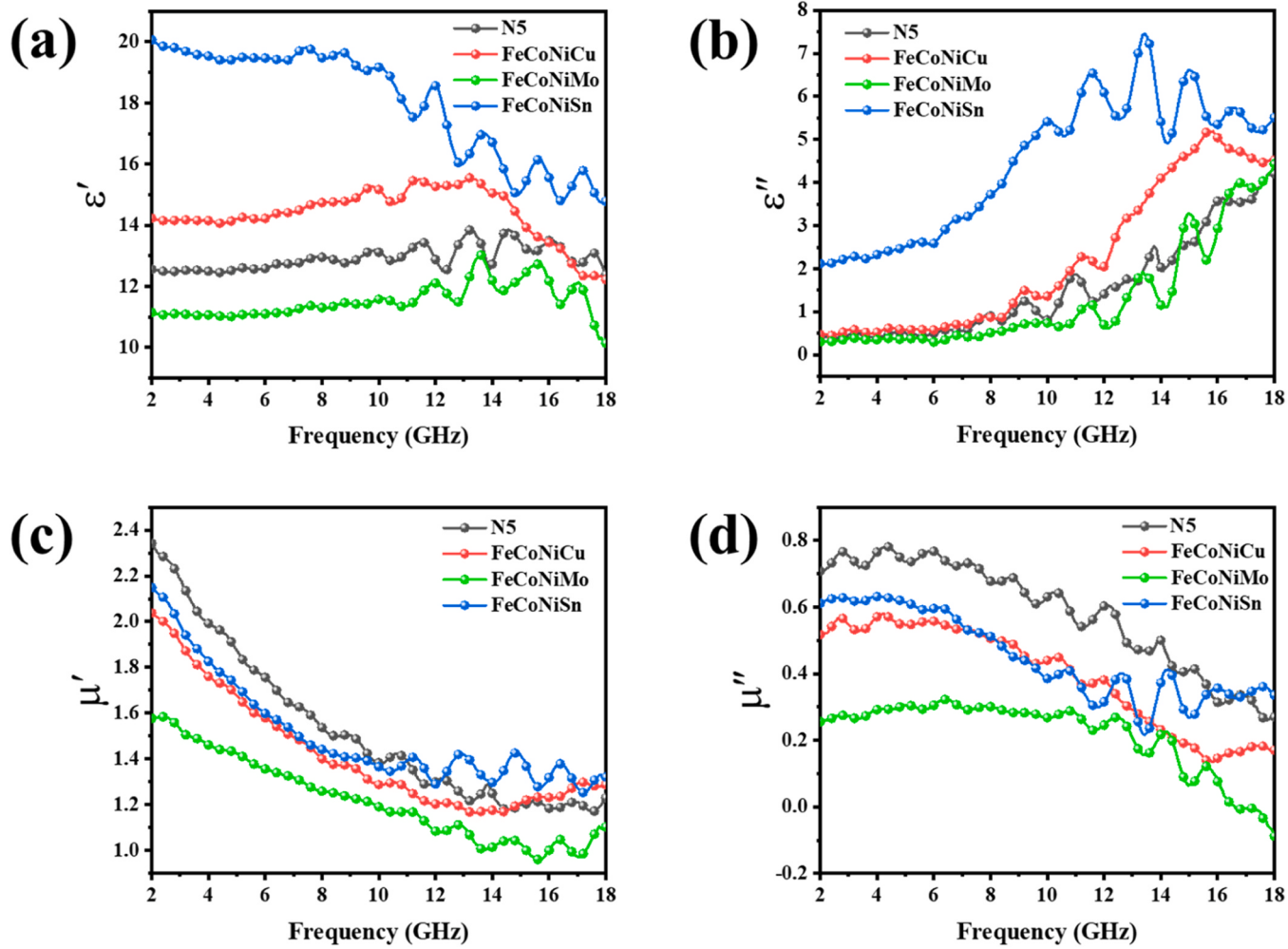


Fig. 5. (a) Real part permittivity, (b) imaginary part permittivity, (c) real part permeability, and (d) imaginary part permeability of N5, FeCoNiCu, FeCoNiMo, and FeCoNiSn.

0, 0.25, 0.5, 0.75, 1, 1.25, 1.5) show a tendency of increasing and then decreasing with the increase of Ni content in the range of 2–8 GHz, the ϵ' values for the N1 sample is the lowest at about 6, and the ϵ'' values for the N3 sample is the highest at about 18. Therefore, the $\text{Fe}_5\text{Co}_4\text{Ni}_x(x = 0, 0.25, 0.5, 0.75, 1, 1.25, 1.5)$ can maintain a certain dielectric loss generated by polarization relaxation in the range of 2–8 GHz, and the content of Ni affects the strength of the dielectric loss. As shown in Fig. 4b, the ϵ'' values of N2, N3, N4, N5, N6, and N7 all show a significant upward trend with the increase of frequency, especially in the high frequency phase of 8–18 GHz show a speedy rising trend. However, the ϵ'' value of N1 maintains basically a steady state with the increase of frequency. It can be inferred that the addition of Ni element in the alloy can increase the electric loss in the high frequency stage (8–18 GHz). Fig. 4c shows that the μ' values of $\text{Fe}_5\text{Co}_4\text{Ni}_x(x = 0, 0.25, 0.5, 0.75, 1, 1.25, 1.5)$ all exhibit a decrease with increasing frequency. Among them, the μ' values of N1 sample is significantly lower than that of other samples in the frequency range of 2–18 GHz, which is shown that the addition of Ni in the preparation can effectively improve the magnetic properties of the alloy. Thus, the magnetic loss capacity of the alloy is improved. The μ'' values of $\text{Fe}_5\text{Co}_4\text{Ni}_x(x = 0, 0.25, 0.5, 0.75, 1, 1.25, 1.5)$ all showed a decreasing trend with the increase of frequency (Fig. 4d). It is speculated that from low frequency to high frequency band, the magnetic loss of the alloy gradually changes from ferromagnetic resonance to eddy current loss [37,38].

As shown in the Fig. 5(a-d), in the frequency range 2–18 GHz, the ϵ' and ϵ'' values of FeCoNiSn is higher than N5, which indicates that the

addition of Sn may be beneficial to the improvement of electrical conductivity. The μ' and μ'' values of FeCoNiCu is close to the N5, the FeCoNiCu still maintains a high magnetism, and above 14 GHz the μ' values of instead shows an upward trend. The ϵ' and ϵ'' values of FeCoNiCu is slightly enhanced, probably due to the high electrical conductivity of Cu. The dielectric permittivity and permeability of FeCoNiMo are significantly lower than those of the original N5, especially in the permeability, which is thought to be caused by the higher doping content of Mo (Tab. S1).

Fig. 6(a-c) shows the reflection loss of N2, N5 and N7 in the frequency range of 2–18 GHz. As the thickness increases, the EAB of N2, N5, and N7 all moved from high frequency to low frequency. And from N2 to N7, the EAB increases and moves to higher frequency, the N7 has the strongest RL reaches 58 GHz at a thickness of 2 mm (Fig. 6c), and the maximum EAB of 7 GHz with thickness of 1.5 mm (Fig. 6g). In the case of maintaining the FeCoNi BCC structure, the increase in Ni content causes a decrease in conductivity and an improvement in dielectric polarization, resulting in the change of the EAB. Fig. 6(d-f) show the reflection loss of quaternary alloys consisting of N5 as matrix doped with Cu, Mo and Sn elements. In comparison with the wave-absorbing properties of the original N5 (Fig. 6b), the wave-absorbing properties of the FeCoNiCu alloy powder with Cu addition did not significantly change (Fig. 6d). The EAB of Mo-doped FeCoNiMo is moved to high frequency and the bandwidth is increased at 1.5 mm thickness (Fig. 6h). After a small amount of Sn is doped, the EAB is moved to lower frequency and the bandwidth is reduced (Fig. 6f).

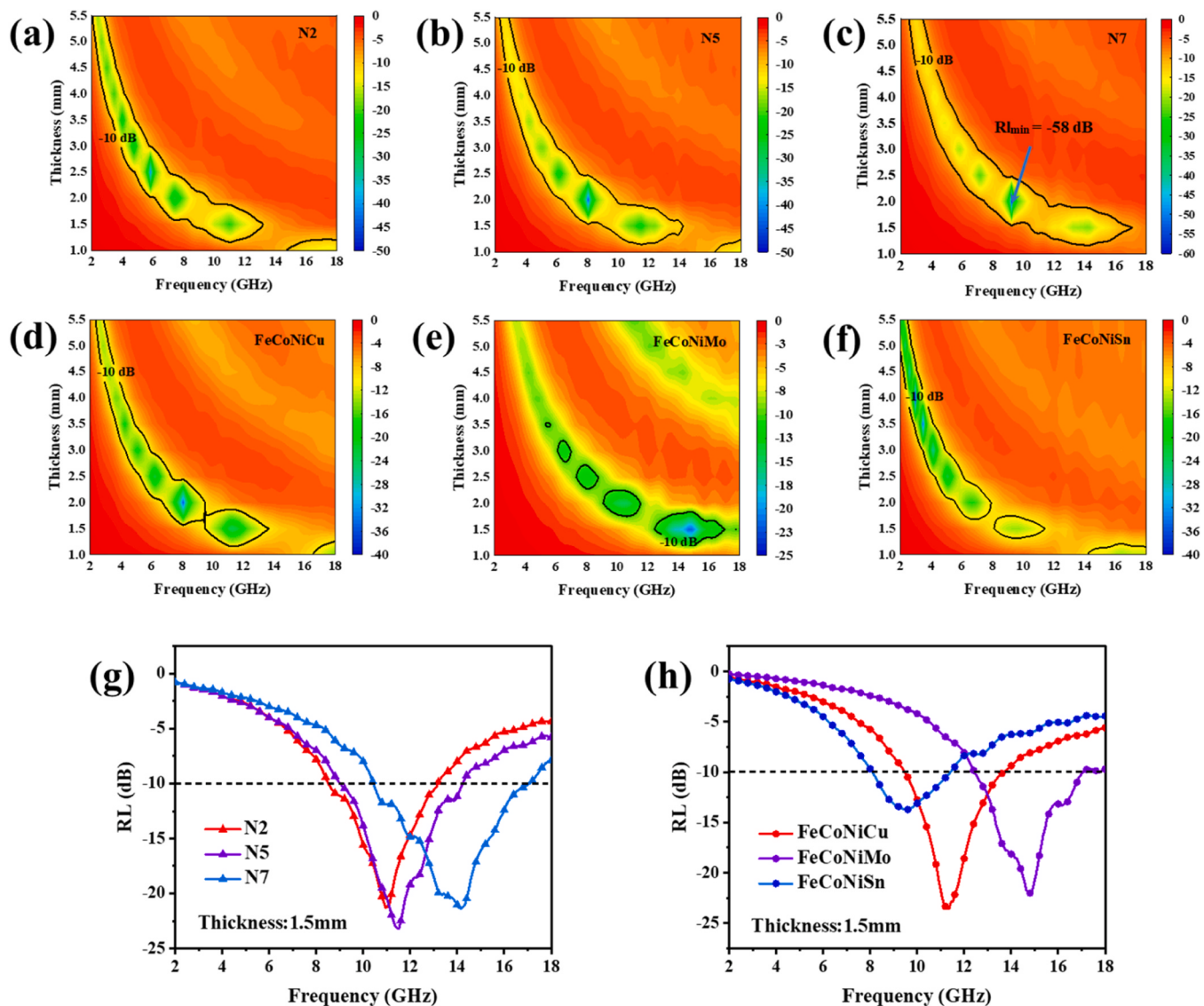


Fig. 6. (a - f) 3D representations of reflection loss (RL) values of (a) N2, (b) N5, (c) N7, (d) FeCoNiCu, (e) FeCoNiMo, (f) FeCoNiSn. (g) The RL-Frequency curves of N2, N5, and N7 at 2 mm thickness. (h) The RL-Frequency curves of FeCoNiCu, FeCoNiMo, and FeCoNiSn at 2 mm thickness.

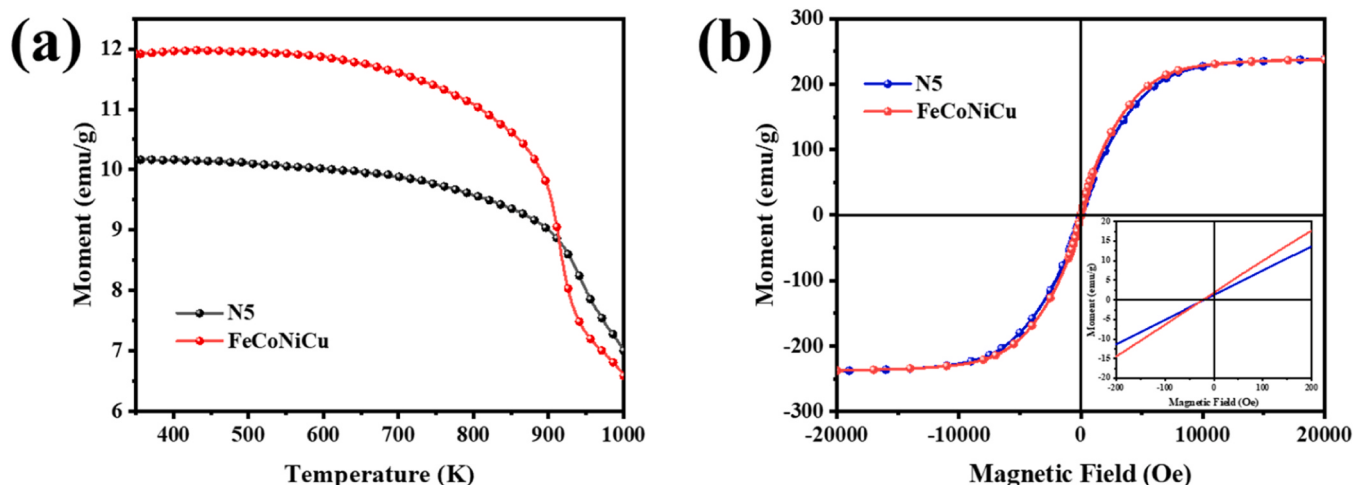


Fig. 7. (a) Magnetic Moment-Temperature curves of N5 and FeCoNiCu; (b) VSM test curves of N5 and FeCoNiCu.

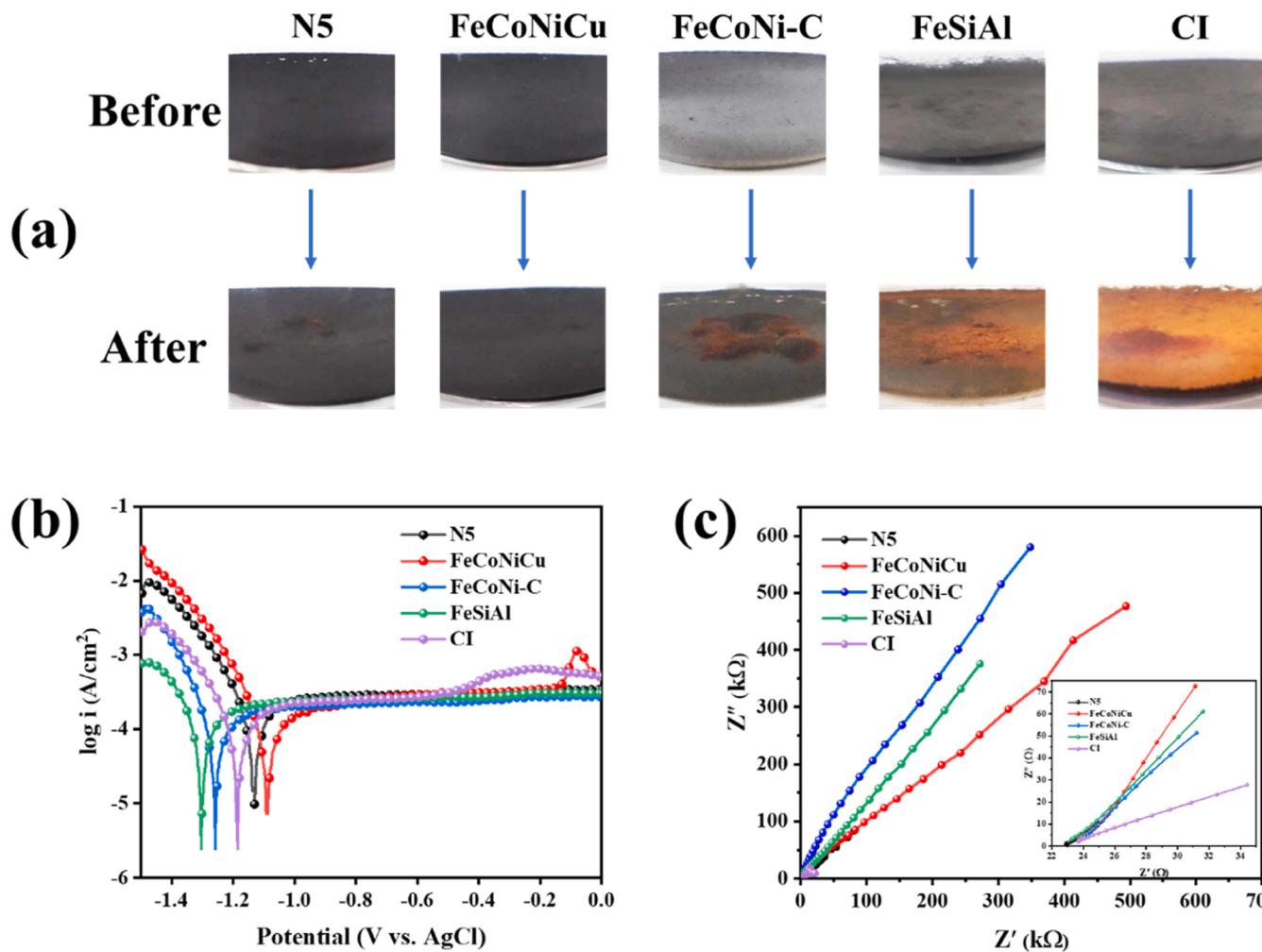


Fig. 8. (a) Appearance of N5, FeCoNiCu, FeCoNi-C, FeSiAl and carbonyl iron before and after 6 months in salt water; (b) Tafel plot and (c) Nyquist plot of N5, FeCoNiCu, FeCoNi-C, FeSiAl and carbonyl iron.

3.4. High temperature magnetism and corrosion resistance

The magnetization strength of N5 and Cu-doped FeCoNiCu was tested at high temperatures, as demonstrated by the curve in Fig. 7a. The sample was subjected to an applied magnetic field strength of 100 Oe while the temperature range rose from 350 K to 1000 K. The N5 possesses a Curie temperature of 940 K, enabling it to maintain magnetism in certain high-temperature situations. As a result, it can sustain the magnetic loss function of electromagnetic waves at elevated temperatures, satisfying the requirement for high-temperature wave absorption to some degree. The Curie temperature of FeCoNiCu alloy formed by doping a small amount of Cu is still maintained above 900 K. However, at a magnetic field of 100 Oe and below 900 K, the magnetization strength of FeCoNiCu is higher than that of N5, which results in relatively strong actual magnetic loss. Fig. 7b demonstrates that the saturation magnetization strength of both N5 and FeCoNiCu reaches 237 emu/g, and their ferromagnetism is improved with respect to the metal monomers, from which it can be seen that FeCoNiCu possesses a better soft magnetism compared to N5, and that the increase in the magnetic susceptibility is conducive to the generation of more natural resonance losses in the high frequency band, which means that FeCoNiCu can maintain a certain magnetic loss function at high temperature below 900 K.

Salt water corrosion resistance tests were conducted on N5, FeCoNiCu and commercially available FeCoNi-C (prepared by atomization method), FeSiAl, and carbonyl iron powder (denoted as CI). 3.5% NaCl

solution was used to simulate the concentration of seawater and the samples were soaked at normal temperature. Fig. 8a shows the changes of several powders after 6 months of immersion in salt water. FeCoNi-C, FeSiAl and CI all incurred large areas of corrosion, but the N5 prepared in this paper shows only a little sign of corrosion. It is worth noting that only FeCoNiCu was not observed to show significant traces of corrosion.

Fig. 8b shows the Tafel curves obtained after the potentiodynamic polarization test, and the corrosion potentials (E_{corr}) of N5, FeCoNiCu, FeCoNi-C, FeSiAl, and CI were obtained by Tafel extrapolation to be -1.132 , -1.093 , -1.258 , -1.296 , and -1.186 V, respectively, and the corrosion current densities (I_{corr}) were 1.180×10^{-4} , 8.339×10^{-5} , 8.653×10^{-5} , 9.322×10^{-5} and 8.672×10^{-5} A. Generally speaking, the corrosion potential determines whether corrosion starts to occur, and the corrosion current reflects the speed of corrosion. Therefore, the material with higher corrosion potential and lower corrosion current exhibits better corrosion resistance. Taken with a comprehensive view, the corrosion potentials of N5 and FeCoNiCu prepared in this paper are significantly higher than those of other samples, in which FeCoNiCu has the highest corrosion potential and the lowest corrosion current. In addition, the Nyquist plot (Fig. 8c) obtained by the EIS test shows that FeCoNiCu has a larger capacitive arc radius. The above test results show that N5 has relatively excellent corrosion resistance, and the FeCoNiCu obtained after incorporation of Cu can show better corrosion resistance.

4. Conclusions

In this paper, binary and ternary nano-alloy powders with Fe, Co, and Ni as components were prepared by wet chemical method, and Cu, Mo, and Sn elements were doped to form quaternary alloys by the method of substitution. The addition of Ni to binary FeCo alloys allows the formation of regularly shaped spheres with dimensions of about 400 nm, and different Ni contents have an effect on the particle size and electromagnetic parameters, thus changing the wave-absorbing properties. Alloying three ferromagnetic metals also provides excellent corrosion resistance, and the high temperature magnetism allows it to maintain a certain wave absorption performance in high temperature scenarios. The quaternary alloy (FeCoNiCu) has superior corrosion resistance and also maintains the original wave-absorbing properties. Overall, this paper invents a universal method to prepare FeCoNi nano-alloy powder and can be doped with Cu, Mo, Sn elements by substitution method, which possesses excellent environmental stability and wave-absorbing properties, and provides a new route of consideration for the preparation of nano high-entropy microwave absorbing alloys.

CRediT authorship contribution statement

Gangjie Lian: Investigation. **Jianhui Yuan:** Supervision, Methodology, Investigation. **Zhilin Zhang:** Writing – review & editing, Writing – original draft, Methodology, Investigation. **Wenbin You:** Supervision, Conceptualization. **Rui Chen:** Investigation. **Yanfang Du:** Validation, Software, Investigation. **Sue Ren:** Methodology, Investigation. **Ren-Chao Che:** Writing – review & editing, Supervision, Conceptualization.

Declaration of Competing Interest

The authors declare that they have no known competing financial interests or personal relationships that could have appeared to influence the work reported in this paper.

Data availability

Data will be made available on request.

Acknowledgements

This work was supported by the National Natural Science Foundation of China (52231007, 12327804, T2321003, 22088101), the Ministry of Science and Technology of China (973 project No. 2021YFA1200600), the Science and Technology Research Project of Jiangxi Provincial Department of Education (GJJ200338), Key Research Project of Zhejiang Lab (No. 2021PE0AC02), the “Chenguang Program” by Shanghai Education Development Foundation and Shanghai Municipal Education Commission (No. 21CGA04), the Fund of Science and Technology on Surface Physics and Chemistry Laboratory (No. JCKYS2023120201), Class III Peak Discipline of Shanghai—Materials Science and Engineering (High-Energy Beam Intelligent Processing and Green Manufacturing), and sponsored by Shanghai Sailing Program (No. 21YF1401800).

Appendix A. Supporting information

Supplementary data associated with this article can be found in the online version at [doi:10.1016/j.jallcom.2024.174175](https://doi.org/10.1016/j.jallcom.2024.174175).

References

- [1] H. Lv, Z. Yang, H. Pan, R. Wu, Electromagnetic absorption materials: current progress and new frontiers, *Prog. Mater. Sci.* 127 (2022) 100946, <https://doi.org/10.1016/j.pmatsci.2022.100946>.
- [2] M. Qin, L. Zhang, H. Wu, Dielectric loss mechanism in electromagnetic wave absorbing materials, *Adv. Sci.* 9 (2022) 2105553, <https://doi.org/10.1002/advs.20210553>.
- [3] Q. Zhang, Z. Du, M. Hou, Z. Ding, X. Huang, A. Chen, Y. Ma, S. Lu, X.-Z. Tang, Ultralight, anisotropic, and self-supported graphene/MWCNT aerogel with high-performance microwave absorption, *Carbon* 188 (2022) 442–452, <https://doi.org/10.1016/j.carbon.2021.11.047>.
- [4] I. Belyaev, C. Blackman, K. Chamberlin, A. DeSalles, S. Dasdag, C. Fernandez, L. Hardell, P. Heroux, E. Kelley, K. Kesari, D. Maisch, E. Mallery-Blythe, R. L. Melnick, A. Miller, J.M. Moskowitz, W. Sun, I. Yakymenko, E. Int Commission Biol Effects, Scientific evidence invalidates health assumptions underlying the FCC and ICNIRP exposure limit determinations for radiofrequency radiation: implications for 5G, *Environ. Health* 21 (2022) 92, <https://doi.org/10.1186/s12940-022-00900-9>.
- [5] B. Dai, Y. Ma, F. Dong, J. Yu, M. Ma, H.K. Thabet, S.M. El-Bahy, M.M. Ibrahim, M. Huang, I. Seok, G. Roymahapatra, N. Naik, B.B. Xu, J. Ding, T. Li, Overview of MXene and conducting polymer matrix composites for electromagnetic wave absorption, *Adv. Compos. Hybrid. Mater.* 5 (2022) 704–754, <https://doi.org/10.1007/s42114-022-00510-6>.
- [6] X. Chen, Y. Huang, K. Zhang, Cobalt nanofibers coated with layered nickel silicate coaxial core-shell composites as excellent anode materials for lithium ion batteries, *J. Colloid Interface Sci.* 513 (2018) 788–796, <https://doi.org/10.1016/j.jcis.2017.11.078>.
- [7] Y. Liu, T. Cui, T. Wu, Y. Li, G. Tong, Excellent microwave-absorbing properties of elliptical Fe₃O₄ nanorings made by a rapid microwave-assisted hydrothermal approach, *Nanotechnology* 27 (2016) 165707, <https://doi.org/10.1088/0957-4484/27/16/165707>.
- [8] G. Tong, Y. Liu, T. Cui, Y. Li, Y. Zhao, J. Guan, Tunable dielectric properties and excellent microwave absorbing properties of elliptical Fe₃O₄ nanorings, *Appl. Phys. Lett.* 108 (2016) 072905, <https://doi.org/10.1063/1.4942095>.
- [9] T.D. Thanh, N. Tran, N.T.V. Chinh, N.T.N. Anh, D.H. Manh, N.Q. Tuan, Excellent microwave absorption performances of cobalt-doped SrFe₁₂O₁₉ hexaferrite with varying incident angles, *J. Alloy. Compd.* 952 (2023), <https://doi.org/10.1016/j.jallcom.2023.170060>.
- [10] T.D. Thanh, N. Tran, N.T.V. Chinh, T.T.H. Giang, D.H. Manh, N.Q. Tuan, Development of high-efficiency tri-layer microwave absorbing materials based on SrMeFe₁₁O₁₉ hexaferrite, *J. Alloy. Compd.* 970 (2024), <https://doi.org/10.1016/j.jallcom.2023.172421>.
- [11] P.T. Tho, N. Tran, N.Q. Tuan, T.A. Ho, C.T.A. Xuan, H.N. Toan, B.W. Lee, Detailed microwave loss mechanisms for nanocomposites of La-doped BaFe₁₂O₁₉ and polyaniiline, *Ceram. Int.* 49 (2023) 23669–23679, <https://doi.org/10.1016/j.ceramint.2023.04.201>.
- [12] C.T.A. Xuan, P.T. Tho, T.Q. Dat, N.V. Khien, T.N. Bach, N.T.M. Hong, T.A. Ho, D. T. Khan, H.N. Toan, N. Tran, Development of high-efficiency microwave absorption properties of La_{1.5}Sr_{0.5}NiO₄ and SrFe₁₂O₁₉-based materials composites, *Surf. Interfaces* 39 (2023), <https://doi.org/10.1016/j.surfin.2023.102890>.
- [13] L. Jia, L. Jiang, W. Zheng, J. Wu, J. Feng, Function of Si on the high-temperature oxidation of FeCoNiMnSi_x HEAs with excellent electromagnetic-wave absorption properties, *J. Alloy. Compd.* 950 (2023) 169853, <https://doi.org/10.1016/j.jallcom.2023.169853>.
- [14] J. Yang, Z. Liu, H. Zhou, L. Jia, A. Wu, L. Jiang, Enhanced electromagnetic-wave absorbing performances and corrosion resistance via tuning Ti contents in FeCoNiCuTi_x high-entropy alloys, *ACS Appl. Mater. Interfaces* 14 (2022) 12375–12384, <https://doi.org/10.1021/acsami.1c25079>.
- [15] H. Zhou, L. Jiang, L. Jia, S. Zhu, L. Wang, A. Wu, X. Zhang, Interstitial boron-doped FeCoNiCr high entropy alloys with excellent electromagnetic-wave absorption and resistance to harsh environments, *J. Alloy. Compd.* 959 (2023) 170579, <https://doi.org/10.1016/j.jallcom.2023.170579>.
- [16] H. Zhou, L. Jiang, S. Zhu, L. Wang, Y. Hu, X. Zhang, A. Wu, Excellent electromagnetic-wave absorbing performances and great harsh-environment resistance of FeCoNiCr_xMn high entropy alloys, *J. Alloy. Compd.* 936 (2023) 168282, <https://doi.org/10.1016/j.jallcom.2022.168282>.
- [17] X. Cao, Z. Jia, D. Hu, G. Wu, Synergistic construction of three-dimensional conductive network and double heterointerface polarization via magnetic FeNi for broadband microwave absorption, *Adv. Compos. Hybrid. Mater.* 5 (2022) 1030–1043, <https://doi.org/10.1007/s42114-021-00415-w>.
- [18] Y. Han, M. He, J. Hu, P. Liu, Z. Liu, Z. Ma, W. Ju, J. Gu, Hierarchical design of FeCo-based microchains for enhanced microwave absorption in C band, *Nano Res.* 16 (2023) 1773–1778, <https://doi.org/10.1007/s12274-022-5111-y>.
- [19] L. Sun, Z. Jia, S. Xu, M. Ling, D. Hu, X. Liu, C. Zhang, G. Wu, Synthesis of NiCo_{2-0.5}Cr₂O₃@C nanoparticles based on hydroxide with the heterogeneous interface for excellent electromagnetic wave absorption properties, *Compos. Commun.* 29 (2022) 100993, <https://doi.org/10.1016/j.coco.2021.100993>.
- [20] Y. Cheng, G. Ji, Z. Li, H. Lv, W. Liu, Y. Zhao, J. Cao, Y. Du, Facile synthesis of FeCo alloys with excellent microwave absorption in the whole Ku-band: Effect of Fe/Co atomic ratio, *J. Alloy. Compd.* 704 (2017) 289–295, <https://doi.org/10.1016/j.jallcom.2017.02.024>.
- [21] S. Li, Y. Huang, N. Zhang, M. Zong, P. Liu, Synthesis of polypyrrole decorated FeCo@SiO₂ as a high-performance electromagnetic absorption material, *J. Alloy. Compd.* 774 (2019) 532–539, <https://doi.org/10.1016/j.jallcom.2018.09.349>.
- [22] B. Liang, S. Wang, D. Kuang, L. Hou, B. Yu, L. Lin, L. Deng, H. Huang, J. He, Facile synthesis and excellent microwave absorption properties of FeCo-C core-shell nanoparticles, *Nanotechnology* 29 (2018) 085604, <https://doi.org/10.1088/1361-6528/aaa52f>.
- [23] M. Rahimi-Nasrabadi, M.H. Mokarian, M.R. Ganjali, M.A. Kashi, S.A. Arani, Synthesis, characterization, magnetic and microwave absorption properties of iron-

- cobalt nanoparticles and iron-cobalt @ polyaniline (FeCo@PANI) nanocomposites, *J. Mater. Sci. Mater. Electron.* 29 (2018) 12126–12134, <https://doi.org/10.1007/s10854-018-9320-9>.
- [24] M.H. Xu, W. Zhong, Z.H. Wang, C. Au, Y.W. Du, Highly stable FeCo/carbon composites: magnetic properties and microwave response, *Phys. E Low. Dimens. Syst. Nanostruct.* 52 (2013) 14–20, <https://doi.org/10.1016/j.physe.2013.03.032>.
- [25] J. Yan, Y. Huang, P. Liu, C. Wei, Large-scale controlled synthesis of magnetic FeCo alloy with different morphologies and their high performance of electromagnetic wave absorption, *J. Mater. Sci. Mater. Electron.* 28 (2017) 3159–3167, <https://doi.org/10.1007/s10854-016-5904-4>.
- [26] J. Zhou, X. Shu, Z. Wang, Y. Liu, Y. Wang, C. Zhou, L. Kong, Hydrothermal synthesis of polyhedral FeCo alloys with enhanced electromagnetic absorption performances, *J. Alloy. Compd.* 794 (2019) 68–75, <https://doi.org/10.1016/j.jallcom.2019.04.217>.
- [27] Y. Zhu, X. Li, P. Chen, B. Zhu, Synthesis, oxidation resistance and microwave absorbing properties of FeCo-based heterostructures, *Ceram. Int.* 46 (2020) 23985–23996, <https://doi.org/10.1016/j.ceramint.2020.06.175>.
- [28] P. Mou, J. Zhao, G. Wang, S. Shi, G. Wan, M. Zhou, Z. Deng, S. Teng, G. Wang, BCN nanosheets derived from coconut shells with outstanding microwave absorption and thermal conductive properties, *Chem. Eng. J.* 437 (2022) 135285, <https://doi.org/10.1016/j.cej.2022.135285>.
- [29] M. Qin, L. Zhang, X. Zhao, H. Wu, Lightweight Ni foam-based ultra-broadband electromagnetic wave absorber, *Adv. Funct. Mater.* 31 (2021) 2103436, <https://doi.org/10.1002/adfm.202103436>.
- [30] Z. Wu, H.-W. Cheng, C. Jin, B. Yang, C. Xu, K. Pei, H. Zhang, Z. Yang, R. Che, Dimensional design and core-shell engineering of nanomaterials for electromagnetic wave absorption, *Adv. Mater.* 34 (2022) 2107538, <https://doi.org/10.1002/adma.202107538>.
- [31] P. Yin, G. Wu, Y. Tang, S. Liu, Y. Zhang, G. Bu, J. Dai, Y. Zhao, Y. Liu, Structure regulation in N-doping biconical carbon frame decorated with CoFe₂O₄ and (Fe,Ni) for broadband microwave absorption, *Chem. Eng. J.* 446 (2022) 136975, <https://doi.org/10.1016/j.cej.2022.136975>.
- [32] M. Green, X. Chen, Recent progress of nanomaterials for microwave absorption, *J. Mater.* 5 (2019) 503–541, <https://doi.org/10.1016/j.jmat.2019.07.003>.
- [33] Z. Xu, Y. Du, D. Liu, Y. Wang, W. Ma, Y. Wang, P. Xu, X. Han, Pea-like Fe/Fe₃C nanoparticles embedded in nitrogen-doped carbon nanotubes with tunable dielectric/magnetic loss and efficient electromagnetic absorption, *ACS Appl. Mater. Interfaces* 11 (2019) 4268–4277, <https://doi.org/10.1021/acsmami.8b19201>.
- [34] A. Drmota, J. Koselj, M. Drofenik, A. Znidarsic, Electromagnetic wave absorption of polymeric nanocomposites based on ferrite with a spinel and hexagonal crystal structure, *J. Magn. Magn. Mater.* 324 (2012) 1225–1229, <https://doi.org/10.1016/j.jmmm.2011.11.015>.
- [35] X. Jiang, H. Niu, J. Li, M. Li, C. Ma, R. Zhang, H. Wang, H. Lu, H. Xu, B. Fan, Construction of core-shell structured SiO₂@MoS₂ nanospheres for broadband electromagnetic wave absorption, *Appl. Surf. Sci.* 628 (2023), <https://doi.org/10.1016/j.apsusc.2023.157355>.
- [36] L. Song, C. Wu, Q. Zhi, F. Zhang, B. Song, L. Guan, Y. Chen, H. Wang, R. Zhang, B. Fan, Multifunctional SiC aerogel reinforced with nanofibers and nanowires for high-efficiency electromagnetic wave absorption, *Chem. Eng. J.* 467 (2023), <https://doi.org/10.1016/j.cej.2023.143518>.
- [37] C. Wu, F. Zhang, Q. Zhi, B. Song, Y. Chen, H. Wang, R. Zhang, H. Li, B. Fan, From binary to ternary and back to binary: transition of electromagnetic wave shielding to absorption among MAB phase Ni₃ZnB₂ and corresponding binary borides Ni_{n+1}B_n(n=1,3), *J. Adv. Ceram* 12 (2023) 2101–2111, <https://doi.org/10.26599/jac.2023.9220812>.
- [38] H. Niu, X. Jiang, W. Li, Z. Min, B.R. Putra, W.T. Wahyuni, H. Wang, R. Zhang, B. Fan, Enhanced electromagnetic wave absorption via optical fiber-like PMMA@Ti₃C₂T_x@SiO₂ composites with improved impedance matching, *Nano Res.* (2023), <https://doi.org/10.1007/s12274-023-6198-5>.